Normal and Shear Forces between Adsorbed and Gelled Layers of Chitosan, a Naturally Occurring Cationic Polyelectrolyte

Nir Kampf,[†] Uri Raviv,[†] and Jacob Klein*[,†,‡]

Department of Materials and Interfaces, Weizmann Institute of Science, Rehovot 76100, Israel, and Physical and Theoretical Chemistry, Oxford University, Oxford OX1 3QZ, U.K.

Received June 13, 2003; Revised Manuscript Received November 12, 2003

ABSTRACT: Using a mica surface force balance, we have measured the interactions between mica surfaces bearing chitosan (a common, naturally occurring, cationic polysaccharide; the average molecular weight of our sample was 6×10^5, degree of deacetylation 85%) adsorbed from acetic acid solution. We also introduced a polyionic cross-linking agent in order to cause gelation of the adsorbed layer. Both normal and shear interactions (the lateral forces acting between the surfaces as they slide past each other under compression) were measured in the two cases (freely adsorbed and cross-linked chitosan layers). Normal interactions between the adsorbed non-cross-linked chitosan layers were similar to previous reports of interactions between such layers; their shear interactions revealed a very low effective friction coefficient μ_{eff} = ca. 0.003 at low compressions, increasing to ca. 0.07 at pressures of some atmospheres. We attribute the low friction to the weak interpenetration between the layers arising from steric effects and counterion osmotic pressures, together with the presence of hydration sheaths about the charged polyelectrolyte segments, which are known to provide efficient local lubrication. The higher friction on strong compressions is attributed to bridging effects. For the case of the cross-linked layer, normal interactions revealed longer ranged and more repulsive forces, due probably to the network formation resulting in a higher effective modulus of the layers. Frictional forces between the rubbing cross-linked layer were much higher than for the non-cross-linked chitosan, an effect we attribute to increased segmental friction arising from attractive interactions between the cross-linking points; this is also consistent with our observation that for the cross-linked layers significant hysteresis was observed when measuring normal interactions on approach and separation of the layers, an effect that was absent for the case of the non-cross-linked adsorbed layers. Refractive index measurements revealed an adsorbance of 1.2 ± 0.4 mg/m^2 of the polymer on each mica surface, consistent with expectations for cationic polymers adsorbed on solid surfaces.

Introduction

Chitosan is a derivative of chitin consisting of β-1,4-*N*-acetylglucosamine[1] (see schematic below). Chitin is widely distributed in nature as a component of the skeletal structure of crustaceans, insects, mushrooms, and the cell wall of fungi,[2,3] and it is the second most widespread natural po1ysaccharide.[4] It may also be viewed as a positively charged polyelectrolyte, and the versatile functions of chitosan have been ascribed to this cationic nature.[5] The present study has a twofold purpose: to study chitosan as a model polyelectrolyte with respect to the way in which it modifies normal and especially shear (i.e., frictional) forces between surfaces onto which it is adsorbed (including in particular the effect of cross-linking the adsorbed layer) and to study these properties with respect to their implications for practical uses of this widely utilized polymer.

For the past two decades, chitosan and its derivatives have drawn considerable attention for its biological properties and potential uses in medical, food industrial, and agricultural fields, mainly due to its extremely low toxicity.[6,7] It is commercially manufactured from chitin (poly-β-(1,4)-*N*-acetyl-D-glucosamin) by heterogeneous alkaline deacetylation using concentrated NaOH solutions[1,5] and is a polysaccharides having an amino group instead of a hydroxyl group on the C2 position of the glucose residue of cellulose.

Chitosan is distinguished from chitin by its solubility in dilute aqueous acid solutions. Its properties in solution depend on molecular weight, the degree of deacetylation, pH, and ionic strength.[8] The pK_a value of the glucosamine segments is 6.3−7.3. As a result of the decreasing charge at higher pH, dissolved chitosan usually flocculates at pH values above about 5.5−6.

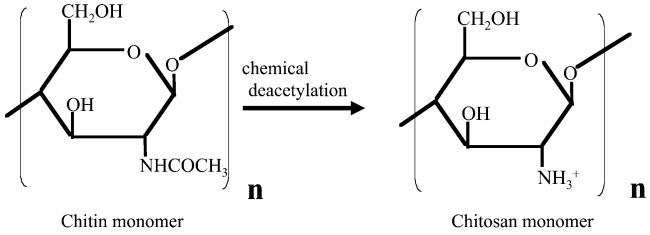

Chitin monomer Chitosan monomer

Chitosan is a cationic polyelectrolyte,[9] being positively charged due to amino groups at acidic pH, to an extent dependent on the degree of deacetylation. It is the only cationic polysaccharide abundantly occurring in nature, while the large majority of other polysaccharides are either neutral or carry a negative charge. In contrast to its food-related and biological studies,[6,7] the rheological properties of concentrated chitosan solutions have scarcely been investigated to date, although a few reports of the properties of its dilute solutions have been published.[10,11] In concentrated solutions chitosan exists in an intermolecular entanglement state.[12]

The gelation mechanism of chitosan is still unclear, and the reports explaining its process are scarce and contradictory.[2,7] The best-understood process for chitosan gelation is via a cross-linking reaction. Chitosan solutions are capable of forming thermally stable gels very rapidly in the presence of an acidic cross-linking agent, such as carboxylic acid, polyphosphates, or other

[†] Weizmann Institute of Science.
[‡] Oxford University.

10.1021/ma0303263 CCC: $27.50
Published on Web 01/20/2004

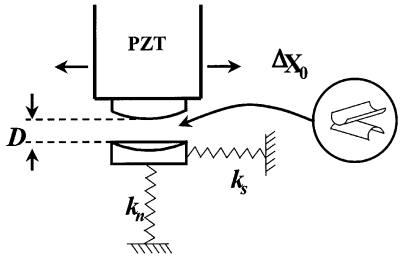

Figure 1. Schematic illustration of the surface force balance equivalent to the actual lens/spring assembly used in our experiments.[20]

negatively charged molecules.[2] Multivalent counterions can be used to cross-link the chitosan in a similar mechanism as used for other polysaccharides such as in alginate gels.[13,14] Among the factors influencing chitosan gel formation are its degree of acetylation, its concentration, the gelation time and temperature, and the cross-linker concentration and type.

While direct measurements of normal force vs distance profiles between adsorbed proteins and polyelectrolytes across aqueous media have been reported,[15,16] including in particular the study of normal surface forces between adsorbed chitosan layers,[4] we are not aware of studies of their shear behavior and the way in which they modify friction. Reports of low friction at different macroscopic gel surfaces have been published[17,18] which describe friction between the surfaces of bulk gels and either a smooth solid or an identical gel surface at low pressures (< ca. 0.1−0.5 atm). A better insight into the frictional processes occurring in biological systems, such as can be found between articular cartilage surfaces, may be achieved by investigating the friction between thin mutually compressed (O(10 atm)) polyelectrolyte gel layers in an aqueous solution environment, and this is one of the aims of the present investigation. We report here the measurement of normal and shear forces between two adsorbed polycationic chitosan layers on solid surfaces, both freely adsorbed and subsequently gelled, using a mica surface force balance (SFB).

Experimental Section

Atomically smooth mica sheets of thickness of ca. 2 μm were prepared by manual cleaving in the standard way from ruby muscovite mica (grade 1, S & J Trading Inc., NY), half-silvered on one side and kept under low-humidity conditions to prevent oxidation of the silver layer prior to an experiment. Two half-silvered mica sheets from the same crystallographic primary facet were then glued to a plano/cylindrical fused silica lens (radius 1 cm) using epoxy resin ("EPON 1004", Shell Chemicals). The mica-coated lenses were mounted in the SFB facing each other in a crossed-cylinder configuration, equivalent to the geometry of a sphere over a flat.

Materials. Chitosan solution (0.065% w/v) was prepared by dissolving chitosan powder (Fluka, high viscosity grade, product no. 48165), having average molecular mass of 6×10^5 g/mol and degree of deacetylation of ca. 85% in 0.04% (v/v) acetic acid solution (pH 3.5). The solution was then stirred overnight at room temperature. Sodium hexametaphosphate (SHMP), or Graham's salt, nominally[19] $(NaPO_3)_6$ (Fluka, Purum grade), was used as the polyanionic cross-linking agent for producing the chitosan gel network. All chemicals were used as received.

Apparatus. The surface force balance (SFB) used in our experiment was similar to that described by Klein and Kumacheva[20] and is shown schematically in Figure 1. White-light multiple-beam interferometry enables measurement of the distance D between the mica surfaces (to ±0.2−0.3 nm) and the geometry of the contact region (including the mean radius of curvature $R \approx 1$ cm) to be determined.

The lower surface is mounted on a horizontal leaf spring (spring constant $k_n = 150$ N/m) whose bending ΔD is measured by interferometry to yield the normal forces $F_n(D)$ with sensitivity ca. ±50 nN. The upper surface is mounted on a four-sectored (+ 1 internal sector) piezo electric tube (PZT) (type Pz29, Ferroperm, Denmark). By applying suitable potentials to different sectors, precisely controlled and highly parallel lateral motion is obtained with respect to the lower surface. In the present experiments shear motion was applied by ramping the potential back and forth (triangular waveform), leading to a motion Δx_0 at uniform velocity in one direction followed by an identical motion in the other. This applied lateral displacement $\Delta x_0(t)$ may have an amplitude of microns while the corresponding change ΔD in normal separation (i.e., deviation from completely parallel motion) is of order 1 nm or less. The PZT is mounted via a rigid stainless steel cradle onto two vertical leaf springs, which are rigidly mounted into the main body of the balance. Shear forces $F_s(D)$ between the surfaces as the upper one is made to move laterally past the lower one are monitored via bending of a set of vertical springs (spring constant $k_s = 300$ N/m) on which the sectored PZT is mounted, determined via changes in an air gap capacitance (Accumeasure ASP-1-ILA, MTI Instruments, NY). This bending $\Delta x(t)$ of the vertical spring is measured to an accuracy ca. ±0.2 nm to yield the shear force as $F_s(D) = k_s \Delta x(t)$.

To minimize ambient vibrations, an electronic vibration isolation system (Halcyonics, MOD-1L, Gottingen, Germany) was used. The noise level in these experiments was higher than reported in some earlier experiments, corresponding to noise in the shear force of ca. ±0.5−1.0 μN, before signal processing. The circuitry of the air gap capacitor may also introduce some high-frequency electronic noise. To improve signal-to-noise, the shear traces were frequency-analyzed (fast Fourier transformed, FFT), and the amplitude of signal at the applied frequency was determined both with the surfaces far apart and at progressively smaller separations. Following subtraction of the systematic error (arising from coupling of the springs to the apparatus via the thin PZT connection wires), it was found that the sensitivity of the shear force measurements, δF_s, corresponding to the scatter of the shear response at the applied frequency, was ca. 30 nN.

Procedure. Calibration of the zero separation ($D = 0$) between the two mica sheets was measured by bringing them into adhesive contact first in air (43% RH, 24 ± 1 °C), then after introducing conductivity water (Milli-Q gradient water purification system, water resistivity 18.2 MΩ, and total organic content < ca. 3−4 ppb), and last in acetic acid (pH = 3.5). Only experiments indicating absence of contaminants by jump-in to adhesive contact were continued for the polysaccharide addition and subsequent force measurements. Further indication of the purity of the system was given by the absence of shear response as the surfaces slid past each other until a jump-in to adhesive contact occurred (see Figure 2), in agreement with ref 26.

After calibration, the bulk of the water in the bath (in which the surfaces were immersed) was replaced by chitosan solution, followed by incubation for 12 ± 2 h. Normal forces were then measured in the presence of chitosan in the solution. Excess chitosan was then removed by replacing the chitosan solution 2−3 times by conductivity water adjusted to pH = 3.5 (by acetic acid). After measuring the normal and shear forces between the freely adsorbed chitosan layers, the surfaces were widely separated ($D \sim 3$ mm) and 12 mL of the liquid was replaced by SHMP cross-linking solution, which was poured in (in a laminar hood environment) between the widely separated mica sheets to create thin cross-linked chitosan film on each mica surface. Since the cross-linking reaction is spontaneous and rapid,[2,13,14] normal and shear measurements were carried out within about 10 min following addition of the cross-linker.

Results shown are from different experiments (different pairs of mica sheets), with data also taken from different

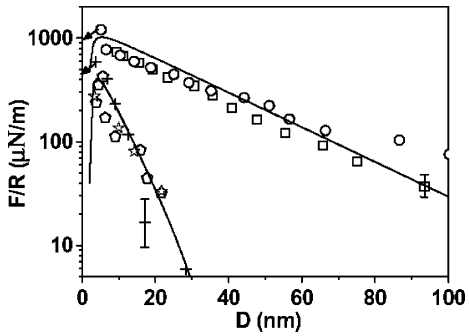

Figure 2. Force ($F_n(D)$) vs distance (D) profiles between mica surfaces across acetic acid (pH 3.5, lower data: different symbols correspond to different runs) and across conductivity water normalized as $F_n(D)/R$ in the Derjaguin approximation, where R is the mean radius of curvature of the surfaces. The zero of separation is with respect to contact in acetic acid. Different symbols represent results from separate experiments. The solid lines are the theoretical DLVO fit to the $F_n(D)/R$ data (see text). The fit corresponds to a Debye lengths (κ^{-1}) of 26 ± 3 nm for the water and 6 ± 1 nm for the acetic acid solution. The calculated effective surface potential (Ψ_0) found to be 76 ± 10 mV in the presence of water and 29 ± 5 mV in acetic acid solution. These values in conductivity water may be a little low for reasons discussed in ref 40. The jump-in occurs when the surfaces approach to within a few nanometers and the hydrated proton counterions condense into the charged surface lattice sites, so that van der Waals attraction becomes dominant.[23]

contact positions between the mica surfaces in each experiment.

Results

Normal Force Profiles. As in earlier studies, we first carried out controls via normal force $F_n(D)$ measurements to establish the integrity of the bare mica surface. This was indicated by long-ranged repulsion across conductivity water, followed by the jump-in from D values of a few nanometers to flat adhesive contact at a surface separation which was of order 0.5−1 nm closer in relative to the air contact position (as shown in Figure 2, top profile), as reported by several previous studies.[21−23] A reduction in the noise level of shear motion, indicated by the output of the air-gap capacitor, was also observed, as expected when the lateral motion of the free surfaces resulting from ambient vibrations was suppressed by their rigid coupling upon jumping to adhesive contact.

Since chitosan solution is obtained by its dissolution in acetic acid, the normal force profiles were determined as controls also across polymer-free acetic acid solution (pH = 3.5), as shown in Figure 2; these were consistent with earlier reports.[4] We also observed that in the acetic acid the jump-in to (from $D = 6 \pm 1$ nm) to flat adhesive contact was to a surface separation D_0 slightly closer in than in conductivity water, and this value was used as the zero of contact for subsequent profiles.

The long-ranged double-layer forces, originating in the osmotic pressure of the counterions trapped between the charged mica surfaces across both water and acetic acid solution, could be fitted by DLVO theory,[24] taking acetic acid as a 1:1 electrolyte solution:[4]

$$F_n(D)/2\pi R = 64Ck_BT\kappa^{-1}\tanh^2(e\psi_0/4k_BT) \times \exp(-\kappa D) - A/12\pi D^2 \quad (1)$$

where C is the electrolyte concentration, T is the temperature (296 ± 1 K), k_B is Boltzmann's constant,

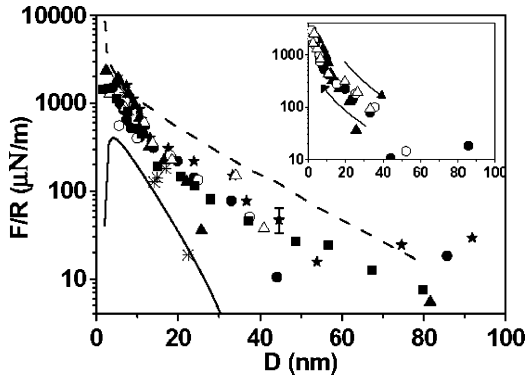

Figure 3. $F_n(D)/R$ vs D profiles in compression between mica surfaces following 12 h of incubation in chitosan (0.06% w/v, pH = 3.5) (filled circles, triangles, and stars); then subsequent to shear (filled squares); and following replacement of solution by exchanging with acetic acid (asterisks). Open symbols indicate force profiles taken at different contact points. The solid line indicates normal force profile in acetic acid (from Figure 2). The broken line is based on the earlier report of normal force profiles of chitosan on mica surfaces by Claesson and Ninham.[4] Inset: normal force−distance profiles between mica surfaces following 12 h incubation in chitosan solution in acetic acid (0.06% w/v, pH = 3.5) in compression (circles for first and triangles for second compression) and in decompression (open symbols) modes.

A is the Hamaker constant of mica across water (2×10^{-20} J), ψ_0 is the effective surface potential, and the κ^{-1} is the Debye length:

$$\kappa^{-1} = (\epsilon k_B T/4\pi\sum_i c_i e_i^2)^{1/2}$$

Here $\epsilon = 80.1$ is the dielectric constant for water, c_i is the concentration of ion "i", and e_i is its charge. Fitting these equations to the force profiles across the acetic acid solution and across conductivity water (solid lines in Figure 2) confirms they have the correct form; the corresponding values of the Debye length and surface potentials are given in the caption to Figure 2. Note that in the case of the acetic acid the protons dissociated from the carboxyl group can readily participate in neutralizing the negatively charged mica, hence reducing the surface potential (and reducing the net repulsion between the surfaces): as expected, both the surface potential and the Debye length were significantly lower for the acid solution relative to conductivity water. A solid−liquid (0.04% acetic acid) surface energy of −1.6 ± 0.5 mN/m was deduced from the force required for pull-off from adhesive contact. This value was lower than that found for water (−2.5 ± 0.7 mN/m) or air (−65 ± 10 mN/m), both of which were comparable to (if somewhat lower than) earlier studies.[23,25,40]

Following these controls, chitosan was added to a concentration 0.065% to the pH 3.5 acetic acid solution and allowed to incubate for 12 ± 2 h, following which normal force−distance profiles $F_n(D)$ between the surfaces were determined; these are shown in Figure 3 (normalized as $F_n(D)/R$). Measurements commenced at a separation $D \cong 350$ nm, and monotonic repulsion (above the scatter of ±30 μN/m) was observed for $D <$ 50 ± 5 nm. The shape and magnitude of these normal force profiles were quite similar to those observed, though at somewhat higher pH value, by Claesson and Ninham[4] for a similar chitosan sample, as shown by the broken line in Figure 3.

Small differences in the measured force were observed between profiles measured on the first approach and

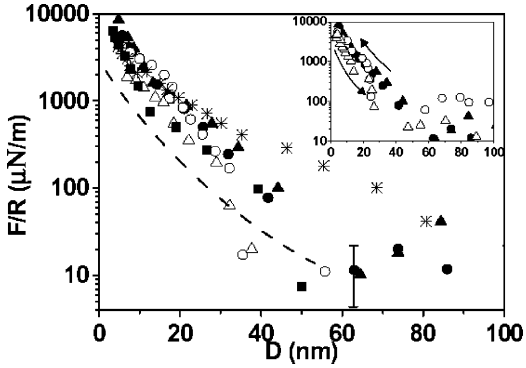

Figure 4. Normal force−distance profiles (compression) between adsorbed chitosan layers following their cross-linking with SHMP (0.01% w/v, pH = 3.5): circles are first compression; triangles are second compression. Filled square symbols and asterisks are profiles following replacement of the SHMP with acetic acid solution (pH = 3.5) and subsequently with conductivity water (pH = 6.0), respectively (the latter is close to the distal-regime profile for conductivity water from Figure 2). Open symbols indicate force profiles taken at different contact points. The broken line is the $F_n(D)/R$ vs D profile between adsorbed chitosan layers prior to cross-linking (from Figure 3). Inset: $F_n(D)/R$ vs D between cross-linked chitosan in compression (circles for first and triangles for second compression) and in decompression (open symbols) modes.

those measured at the successive compressions and between compression−decompression cycles (Figure 3 and inset of Figure 3). These differences were not significantly greater than the scatter (of order 20% on average).

To examine the effect on the normal force profiles of the presence of the chitosan in the bulk solution, the chitosan solution was replaced (as described earlier) with polymer-free acetic acid at the same pH. The subsequently measured $F_n(D)$ profiles were similar to the prewashed ones (different symbols in Figure 3), in agreement with the previous report by Claesson and Ninham[4] and with earlier studies on neutral adsorbed and grafted polymers.[26,27] Clearly, the presence of free polymer between the adsorbed layers makes negligible contribution (being presumably extruded out as the surfaces approach).

The next step was to cross-link the adsorbed chitosan by adding the SHMP cross-linker to concentration 0.01% w/v (pH 3.5). Following the cross-linking, $F_n(D)$ profiles were measured under a range of conditions: in the presence of the added SHMP, then following its replacement by acetic acid solution (pH 3.5) and finally following replacement of the acetic acid by conductivity water; in addition, both compression and decompression profiles were monitored. These profiles are shown in Figure 4 and compared with the mean profile for the non-cross-linked adsorbed chitosan (broken curve). Several features are immediately clear: first, that the presence of the free SHMP itself has little effect (since its removal by washing does not result in large changes to $F_n(D)$); second, that there is a more marked hysteresis between compression and decompression (inset to Figure 4) than for the non-cross-linked layers; and finally, that the cross-linking has led to a significantly stronger and somewhat longer ranged repulsion in comparison to the non-cross-linked adsorbed chitosan. This was particularly marked at the highest compressions. The thicker "hard wall" on strong compression in the cross-linked film may be viewed as indicating a higher effective modulus and will be discussed below.

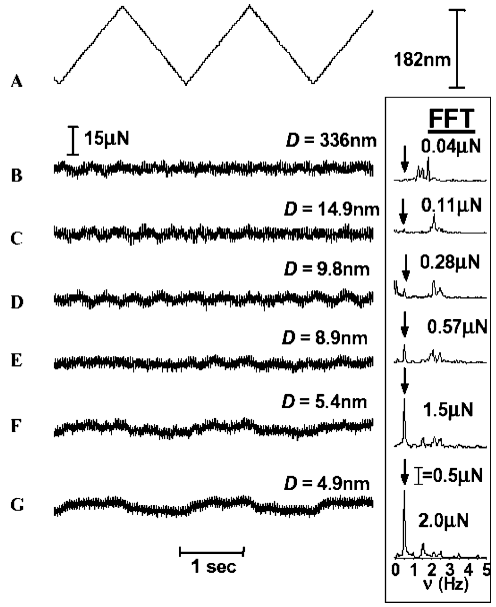

Figure 5. As-recorded oscilloscope traces from shear measurements. Trace A: applied back-and-forth motion to upper surface (amplitude of applied motion vs time). Traces B−G: shear forces transmitted between the surfaces bearing non-cross-linked adsorbed chitosan layers at different surface separations D as indicated, in response to applied motion as in trace A. The right-hand traces are the frequency-dependent shear forces determined by fast Fourier transforms of traces B−G.

Shear Forces. Since normal interactions between adsorbed, non-cross-linked chitosan layers were earlier studied comprehensively,[4] and are in quite close agreement with our results, the main new goals in the present study are the comparative measurement of normal and particularly frictional forces for the two configurations: the adsorbed and the gelled-adsorbed states of the polyelectrolyte. Shear force measurements between the adsorbed and cross-linked chitosan were carried out by applying back-and-forth lateral motion of the top polymer-coated surface with respect to the lower one. The measurements commenced at large surface separations (D > 300 nm) where no normal forces above the scatter could be observed, and typical as-recorded shear force traces are shown in Figure 5 (free adsorbed layers) and Figure 6 (following gelation by the SHMP). Traces A in Figures 5 and 6 show the shear motion $\Delta x_0(t)$ applied to the upper surface as a function of time, while traces B−G are the corresponding shear forces $F_s(t)$ transmitted across the gap between them at different surface separations as shown. On the right-hand of the traces are shown the shear force components as a function of frequency (derived from the fast Fourier transform (FFT) of the traces), with an arrow indicating the drive frequency ω_0 (0.5 Hz). Even for the largest separations, traces B in Figures 5 and 6, where there is no measurable normal interactions between the surfaces, there is still a residual shear force F_{s0} (ω_0) (in the range 30−60 nN, varying between different experiments) measurable at the drive frequency over and above the noise level; this arises from the coupling of the upper surface to the lower one via the thin wires connected to the PZT. This systematic signal (not due to any polymer/polymer interactions) may be subtracted from the actual signal to yield $F_s(D,\omega_0)$, the relevant shear force at the sliding velocity

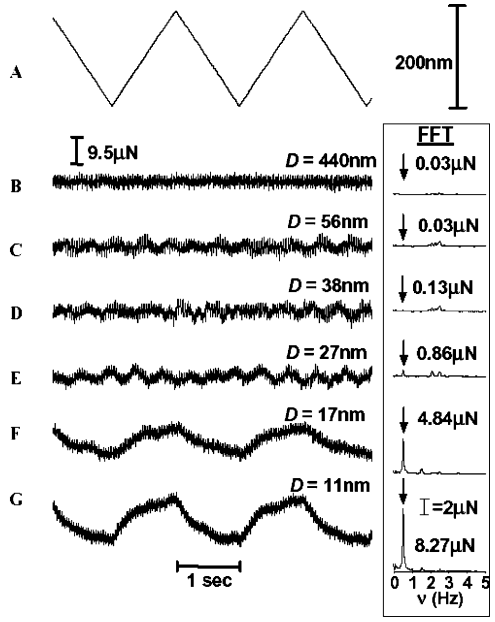

Figure 6. As-recorded oscilloscope traces from shear measurements. Trace A: applied back-and-forth motion to upper surface (amplitude of applied motion vs time). Traces B−G: shear forces transmitted between the surfaces following cross-linking of the adsorbed layers via SHMP, at different surface separations D as indicated, in response to applied motion as in trace A. The right-hand traces are the frequency-dependent shear forces determined by fast Fourier transforms (FFT) of traces B−G.

of the measurements, as revealed in traces C−G in Figures 5 and 6.

For the case of adsorbed non-cross-linked chitosan (Figure 5), the FFT analysis showed that shear forces $F_s(D,\omega_0)$ started to exceed $F_{s0}(\omega_0)$ systematically at D < ca. 20 nm and increased monotonically at lower values (for example, trace G in Figure 5 shows F_s to have a value of some 2 μN at D = 4.9 nm). Following cross-linking (Figure 6), it was found that $F_s(D,\omega_0)$ began to exceed $F_{s0}(\omega_0)$ already at significantly larger separations (D < ca. 35 ± 5 nm) and to increase continuously at lower D values (trace G in Figure 6 illustrates the case of D = 11 nm, where $F_s(\omega_0)$ has attained a value of some 8 μN). We observe that the form of the traces where F_s is clearly developed (e.g., trace G in Figure 5 and traces F, G in Figure 6) shows that the shear forces reach a quasi-plateau value, following a sharp initial rise, and it is this that is taken as the sliding shear force for the particular shear velocity. We should bear in mind that at the highest compressions for the cross-linked layer (e.g., trace G, Figure 6) the plateau was not fully developed over the amplitude of shear motion applied, suggesting the true shear force corresponding to sliding at the particular velocity used may be somewhat higher.

Figure 7 summarizes the $F_s(D)$ vs D variation between chitosan and cross-linked chitosan layers at fixed shear velocity (V_s = 200 nm/s, corresponding to the traces in Figures 5 and 6, together with other data not shown in those figures). The inset to Figure 7 shows the onset of F_s for the non-cross-linked chitosan layers on an expanded scale. The onset of detectable shear forces at the values of D noted above for the two cases is clearly seen, as is their much greater magnitude for the cross-linked case.

To examine further the nature of the frictional drag between the surface-attached layers, shear forces be-

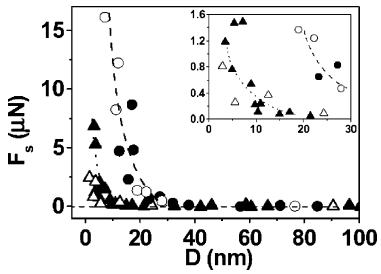

Figure 7. Summary of separation (D) vs shear force ($F_s(D)$) data for non-cross-linked (triangles) and cross-linked chitosan (circles), taken from traces such as shown in Figures 5 and 6. Open and filled symbols show data taken from different experiments. All shear measurements shown were taken at shear velocity V_s = 200 ± 20 nm/s. The inset shows the region of onset of F_s between non-cross-linked layers on a magnified scale.

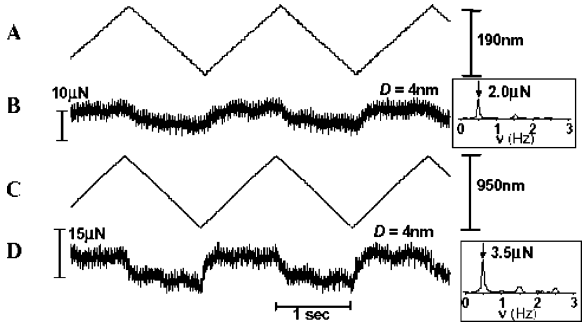

Figure 8. Shear force traces at two different applied shear velocities but at fixed D (4 ± 0.2 nm) between non-cross-linked adsorbed chitosan layers. The applied lateral back-and-forth motion is presented in traces A (V_s = 200 nm/s) and C (V_s = 950 nm/s). The shear responses are shown by traces B and D, respectively. On the right are the frequency-dependent shear forces determined by FFT from traces B and D.

tween the freely adsorbed and between the cross-linked chitosan layers were measured at different shear velocities for a given D. An example of shear force traces for the case of non-cross-linked layers at two different shear velocities differing by a factor of ca. 5, both for the same D value (4 ± 0.2 nm), is shown in Figure 8. Here the shear velocity is varied by increasing the amplitude of the applied motion at a given back-and-forth frequency (1 Hz), traces A and C in Figure 8, while the corresponding $F_s(t)$ traces are shown in traces B and D. The FFT analysis is given in the inset to the right of each shear trace, showing clearly the larger forces at the higher shear velocity; we note that the ca. 75% increase in the shear force is very much weaker than the corresponding 5-fold increase of the shear rate, as discussed further below.

The variation of the shear force with increasing shear rate $\dot{\gamma} = (V_s/D)$ of both freely adsorbed and cross-linked chitosan is presented in Figure 9 for a given surface separation D = 7 ± 1 nm; comparing at one given D value, as in Figure 9, yields the most transparent physical picture. It was observed that, prior to cross-linking, little increase in the shear forces could be measured above the noise level up $\dot{\gamma}$ = ca. 30 s^{-1} (a slight increase in F_s is indicated at higher $\dot{\gamma}$). For the cross-linked adsorbed chitosan layer, a significant increase in the shear force with increasing shear rate starts at lower shear rates (< ca. 10 s^{-1}).

In Figure 10 is plotted the variation of the measured shear forces $F_s(D)$ at different loads $F_n(D)$, determined from the normal force profiles, all at the same shear

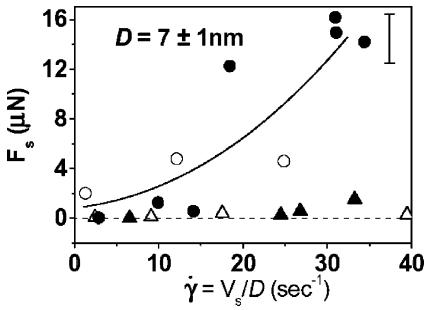

Figure 9. Summary of the shear force (F_s) vs shear rate $\dot{\gamma}$ (= V_s/D) between non-cross-linked (triangles) and cross-linked chitosan (circles), all taken at compressions $D = 7 \pm 1$ nm. Open symbols indicate data taken from different experiments.

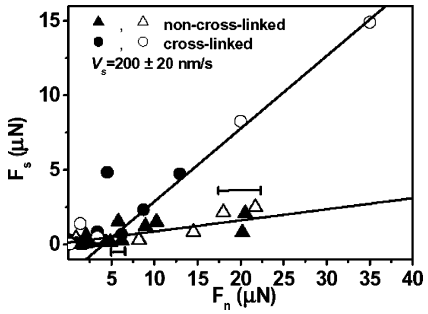

Figure 10. $F_n(D)$ vs $F_s(D)$ for non-cross-linked adsorbed chitosan layers (triangles) and for cross-linked chitosan layers (circles). Open symbols indicate data taken from different experiments. All shear data shown were taken at shear velocity $V_s = 200 \pm 20$ nm/s. Solid lines are a fit to a linear relation between $F_n(D)$ and $F_s(D)$, evaluated for F_s values significantly higher than the error in F_s ($F_s > 0.1$ μN). $F_n(D)$ values are taken from normal force profiles as in Figures 3 and 4 for the surface separations D corresponding to the F_s-(D) data.

velocity (though not of course the same shear rate, which depends for a given velocity on D). A mean friction coefficient μ for the sliding chitosan-coated surfaces prior to cross-linking may be calculated from the slope of the $F_n(D)$ vs $F_s(D)$ plot (Figure 10). This slope however varies with the load (and D), and while its mean value is $\mu \approx 0.07$, an effective friction coefficient μ_{eff} may be defined at different points as $\mu_{eff} = F_s(D)/F_n(D)$. At the onset of measurable shear forces between the sliding non-cross-linked layers, this can take the much lower value $\mu_{eff} \approx 0.003$. For the case of the cross-linked chitosan layers, the mean slope in the linear region of the $F_n(D)$ vs $F_s(D)$ curve is $\mu \approx 0.5$, some 7-fold higher than for the non-cross-linked case, while at the point of onset of measurable shear forces for the gelled layer, $\mu_{eff} \approx 0.01-0.02$.

Refractive Index and Polymer Adsorbance. The refractive index $n(D)$ of the compressed chitosan as a function of separation D was also monitored (via simultaneous measurement of odd and even fringes at the given separations D, as previously described[28]), both for non-cross-linked and for the gelled adsorbed layers. These profiles are shown in Figure 11 and enable the adsorbance Γ of the chitosan (mass adsorbed per unit area of mica surface) to be estimated, using the following linear relationship:

$$n(D) = n_{water} + (2\Gamma/\rho D)(n_{polymer} - n_{water}) \qquad (2)$$

where ρ is the polymer density and $n_{polymer}$ is the refractive index of bulk polyelectrolyte (determined

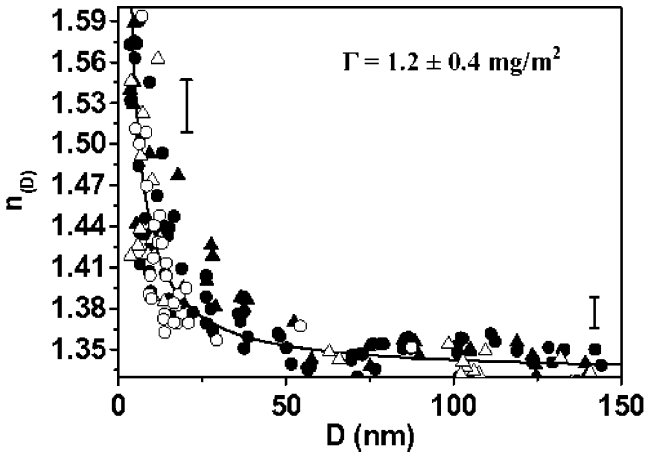

Figure 11. Mean refractive index $n(D)$ of the medium between the mica surfaces in the presence of non-cross-linked (triangles) and cross-linked (circles) chitosan. Open symbols indicate data taken from different experiments. The solid line (a fit to eq 2 in the text) corresponds to an adsorbance $\Gamma = 1.2 \pm 0.4$ mg/m^2 of chitosan on each mica surface.

using an Abbé refactometer; the value obtained, 1.59, is close to that determined in an earlier study[29]). The adsorbance of chitosan estimated using this expression was found to be 1.2 ± 0.4 mg/m^2 (the fit to this value is shown by the solid curve in Figure 11). While there is considerable scatter in the data (not unusual for refractive index measurements, particularly for $D <$ ca. 20 nm), no significant differences in the $n(D)$ profiles of the adsorbed chitosan were observed to result on cross-linking. This result is not surprising since the cross-linking merely gels the previously adsorbed polymer on the surface. Moreover, no differences within the scatter were observed following shear even at the highest compressions, suggesting that little polymer was removed by the shear itself.

Discussion

The main new findings of this study concern the shear forces that act between freely adsorbed chitosan layers and between the same layers once they have undergone cross-linking using the sodium hexametaphosphate (SHMP) linking agent. The normal force−distance F_n-(D) profiles between the adsorbed chitosan layers serve to characterize them, both prior to and following the shear. For the case of the non-cross-linked layers these profiles (Figure 3) resemble fairly closely the normal profiles (broken curve in Figure 3) reported by Claesson and Ninham[4] between similar, though not identical, chitosan samples adsorbed under similar conditions. The structure of the adsorbed chitosan layers was earlier comprehensively analyzed by these authors[4] exclusively on the basis of their $F_n(D)$ profiles; they concluded that their polyelectrolyte adsorbed rather flatly (layer thickness up to a few nanometers). In the present experiments we have measured not only the normal force profiles but also the shear profiles $F_s(D)$, the adsorbance of the polymer Γ, and the effect of cross-linking. Together these provide a more detailed picture, and they all suggest a somewhat thicker adsorbed layer then reported in ref 5 with the largest loops extending to ca. 10−15 nm from each surface, as discussed below. This difference from the earlier results may be due to the different chemistry and size of the chitosan samples (in the Claesson/Ninham paper the molecular weight was $M \approx 7 \times 10^5$, and degree of deacetylation (DA) was

DA ≈ 90−95%, compared with $M \approx 6 \times 10^5$ and DA ≈ 85%, respectively, in the present study) as well as to the slightly different pH used in our experiments.

From the force profiles (Figure 3), marked deviations from double-layer electrostatic interactions between the non-cross-linked adsorbed layers are first observed at surface separations $D_{onset} \approx 15-20$ nm. Since such deviations are likely due to steric repulsion between the opposing segments, one expects that the adsorbed layer thickness is given by $L \cong$ ca. 10 nm ($= D_{onset}/2$) though it is very possible that the largest loops extend beyond that distance, since steric repulsion may not be detectable until some compression has occurred. We note also that the adsorbance Γ of the polyelectrolyte, at 1.2 ± 0.4 mg/m^2, is very much in line with values for other polyelectrolytes on oppositely charged surfaces[29,30] and in the case of the cationic poly-L-lysine on mica was found[31,32] to be 2 mg/m^2.

We note here that one may attempt a DLVO-type fit of the $F_n(D)$ profile between the adsorbed chitosan layers in the far field regime ($D \gg 2L$), stipulating an outer Helmholtz plane at a distance L from each surface. (This corresponds to an assumption that the charge on the polymer segments within the adsorbed layers is fully compensated by mobile counterions within the layer, so that the double-layer repulsion originates in a net charge residing at the surface of the adsorbed layer.) Such a fit would yield an effective surface potential at the adsorbed layer surface. However, bearing in mind the diffuse nature of the adsorbed layer and its power law decay away from the surface, such an outer Helmholtz plane would be difficult to define precisely.

Following cross-linking, both the range of the repulsive interaction and its magnitude increase significantly, as seen in Figure 4. This may be explained qualitatively as follows: For the non-cross-linked layers, initial repulsive interactions may be relatively weak as the adsorbed layers can deform readily (more segments being forced to adsorb, with a consequent gain in free energy thereby reducing the net repulsion expected from osmotic considerations alone[30,31]). Once cross-linking occurs, however, the adsorbed layer becomes gellike and therefore much stiffer, as the deformation on compression can no longer be accommodated by the layer "spreading out" on the mica substrate (segments being constrained in the network to affine positions). This idea fits especially well the much stronger hard-wall repulsion observed with the cross-linked layers. That this stronger repulsion is due to the cross-linking and not say to adsorption of additional polymer is revealed by the refractive index profile (Figure 11), which, within the scatter, suggests little change in the magnitude of the adsorbance Γ on cross-linking. The very low residual concentration of free chitosan in solution following 2−3 washes prior to cross-linker addition also make it unlikely that additional polymer attaches to the surface layer after the SHMP is added.

A further point worth remarking is that the hysteresis on separation is significantly larger for the cross-linked layers than for the non-cross-linked ones. This suggests two things. First, for the non-cross-linked layers, additional segments that are forced on compression to adsorb appear to desorb rapidly on the time scale of the separation (so that hysteresis is weak for that case, in contrast to a previous report,[32] though more in line with other studies on adsorbed polyelectrolytes[15,16]). It is also unlike the marked hysteresis between uncharged adsorbed layers,[33,34] either because of greater repulsion between the charged segments or because of weaker segment−substrate adhesion due to hydration layers around the charges. Second, for the cross-linked layers, where additional segment adsorption on compression is unlikely for the reasons discussed above, the more marked hysteresis may suggest that some interlayer attraction is active, which is long-lived on the time scale of the separation. This attractive interaction may arise from the SMHP cross-linkers if on contact between the cross-linked layers some of the cross-linkers on one layer attach to polyelectrolyte segments on the other layer or interact with cross-linkers on the other layer. This possibility is especially relevant for understanding the shear force measurements between the gelled layers. Another possibility is that cross-links break on compression to re-form more compactly and then take a while to re-form to the equilibrium thickness on decompression.

As noted, the most significant new findings in the present study relate to the frictional or shear forces. This is one of the first reports of frictional forces under controlled conditions between surface-attached polyelectrolytes (the others being an SFB study involving polyelectrolyte brushes[35] and one using AFM to measure forces between very weakly charged adsorbed polyelectrolytes[36]) and the first for naturally occurring polymers. As seen in the as-recorded traces in Figure 5 and in the plots in Figures 7, 9, and 10 (which reveal also the effect of different shear rates), the frictional forces between the sliding, mutually compressed non-cross-linked adsorbed chitosan layers are rather weak. Indeed, at the point at which $F_s(D)$ first becomes measurable above the small systematic signal (due to the PZ wire coupling noted earlier), the effective friction coefficient $\mu_{eff} = F_s(D)/F_n(D)$ is extremely low, $\mu_{eff} \approx 0.003$, increasing at higher compressions to $\mu_{eff} \approx 0.07$. We believe the origin of the very low friction—and correspondingly efficient lubrication—is as follows. When dissolving the chitosan in acetic acid solution, the amino groups are cationized and therefore repel each other.[7] As two such surface-attached chitosan layers come into overlap in the good-solvent conditions of the chitosan/acetic acid solution, excluded-volume effects also come into play, and the extent of interpenetration between them is weak (though not as weak as for the case of polymer brushes in good solvents, where segments cannot gain any free energy by adsorbing on the substrate during compression). This steric effect, which was also observed for neutral adsorbed brushes in a good solvent,[34] is augmented in the case of the polyelectrolytes by the high counterion osmotic pressure within the adsorbed layers; in addition, we believe that a major factor in reducing the segment−segment friction as the layers rub past each other has to do with the hydration layers surrounding each of the charges on the ionized chitosan. Such hydration sheaths have recently been shown[37] to provide extremely efficient lubrication, being fluid on one hand while on the other hand they resist being removed even under high pressure. For this reason such hydrated charges have been likened to "molecular ball-bearings".

At higher compressions the effective shear force increases markedly. This increase is similar to that observed on shear of compressed neutral adsorbed polymer,[34] which was attributed to the onset of bridging effects: When the layers are sufficiently pressed against each other, segments from polymers adsorbed on one

surface may penetrate the other layer to adsorb on the opposing substrate. They thus form bridges; presumably when shear occurs these bridges initially stretch to oppose the sliding motion, and as they are dragged along energy is dissipated. We believe this is the origin of the increased friction also in the present case of adsorbed polyelectrolytes. We note that such bridging effects would not apply for the case of polymer brushes,[38] especially polyelectrolyte brushes, and indeed in the latter case the lubrication has been found to be extremely efficient.[35] It is also of interest to relate this dissipation to the shear rate dependent friction force, as revealed in Figures 8 and 9. Clearly, from the data in Figure 9 there is little increase in F_s over the range of shear rates at the separation ($D = 7 \pm 1$ nm) shown. This indicates that the relevant relaxation rates of the processes controlling F_s for these compressions (i.e., $D = 7$ nm) are of order 30 s^{-1} or faster, which is also be in line with the absence of significant hysteresis on compression/decompression of the surfaces (inset to Figure 3). Note however that at higher compressions of the non-cross-linked polymer layer, as in Figure 8 ($D = 4$ nm), the shear forces are much higher at shear rates only slightly greater ($\dot{\gamma} > 50$ s^{-1}). This is probably due both to the greater extent of bridging at the higher compressions and also to the larger effective viscosity of the layers at the higher densities corresponding to the stronger compressions; the mean volume fraction of the adsorbed layers at $D = 4$ nm is ca. 0.6. That the increased shear forces are not due to increased viscosity alone however can be seen from the shear-rate dependence of F_s: in Figure 8, a 5-fold increase in the shear rate (for $D = 4$ nm) results only in a 75% increase in the shear force, confirming that the frictional drag cannot be purely Newtonian in origin (i.e., due to viscosity alone). This again suggests that a more complex mechanism for the frictional dissipation must be active (possibly a combination of enhanced bridging and entanglement effects within the layers at the highest compressions).

Following cross-linking the picture is very different. In this case significant shear forces are detected already at $D \approx 35$ nm and below, in other words close to initial overlap. This observation is consistent with the idea that the two gelled layers have some adhesive interaction possibly mediated by the SHMP cross-linker, as discussed above. Higher compression brings the gelled layers into more intimate contact, and the shear forces increase correspondingly. In the case of the gelled layers we do not expect bridging to occur—interpenetration of the layers is suppressed by the network-like structure induced by the cross-links, and so precludes bridging. However, dissipation does take place, as these presumed attractive (SMHP-mediated) interactions, to which the hysteresis in $F_n(D)$ above was also attributed, lead to enhanced segmental friction forces between the layers. The shear-rate dependence of F_s for the cross-linked layers (Figure 9, circular symbols) is very roughly linear within the scatter. This would be consistent with a viscous dissipation mechanism as might arise from an increased effective friction coefficient resulting from attractive interactions between cross-link points or mediated by the cross-linker. If this is indeed the mechanism responsible for the higher frictional drag, it implies quite a slow a relaxation rate for the attractive cross-link/cross-link interactions (a high effective viscosity of the sheared gel/gel interfacial layer). This would be in line with the observed hysteresis in the normal force profile on compression/decompression of the cross-linked layers, which also takes place over scales of seconds (inset to Figure 4). It is appropriate finally to recall the extensive studies on friction at bulk gel surfaces carried out by Gong et al.,[17,18] though for several reasons these cannot be directly compared with the present microscopic investigation.

To conclude, we have carried out the first detailed measurements of shear forces between mutually sliding, surface-adsorbed polyelectrolytes under compression. These show that the frictional drag between chitosan, a cationic polysaccharide ubiquitous in nature, adsorbed onto mica substrates, is very weak (μ_{eff} = ca. 0.003) at low pressures. This is attributed to weak interpenetration arising from steric repulsion together with counterion osmotic pressure and to the very weak segmental friction arising from hydration sheaths about the charged segments. At higher pressures the friction increases—though up to several atmospheres the effective friction coefficient is still only ca. 0.07—probably due to bridging effects. We have also cross-linked the adsorbed chitosan layers using a multiply charged anionic linker. This presumably suppresses the bridging—due to affine network formation—but our results suggest that the cross-linkers themselves leads to additional attractive interaction between the layers and consequently also to increased frictional interactions between the gelled layers. We should emphasize in passing that our use of mica does not weaken the generality of our conclusions, since the detailed nature of the surfaces in these experiments does not play a major role in the frictional interactions (which are initially dominated by the polymer/polymer interface). The main role of the mica is in providing an adsorbing substrate for the polyelectrolyte—this determines the strength of the adsorbance and to an extent the layer thickness and also the eventual likelihood of bridging. Finally, it is tempting to relate our results to biological lubrication phenomena,[39] where soft surfaces bearing either charges or charged polymers slide past each other. Care must be taken, however: although we believe that our findings concerning low frictional drag between charged adsorbed layers have general implications for biolubrication, the pressures we have used are somewhat lower than those between articular cartilage in knees and hips, though comparable or larger than those across non-load-bearing surfaces (finger joints, eyelids). We should also bear in mind that mica is a rigid substrate relative to biological surfaces and in addition that the shear rates used in our experiments are much lower than those typical in biolubrication. Nonetheless, we believe some of our conclusions may be relevant to a better understanding of biological lubrication as well as to improving biomedical devices.

References and Notes

(1) Varum, K. M.; Ottoy, M. H.; Smidsrod, O. *Carbohydr. Polym.* **1994**, *25*, 65−70.
(2) Enriquez, L. G.; Flick, G. J. In *Food Emulsifiers*; Charalambous, G. D. G., Ed.; Elsevier Science Publication: New York, 1989.
(3) Knorr, D. *Food Technol.* **1991**, *45*, 114−122.
(4) Claesson, P. M.; Ninham, B. W. *Langmuir* **1992**, *8*, 1406−1412.
(5) Muzzarelli, R. A. A. *Carbohydr. Polym.* **1996**, *29*, 309−316.
(6) Li, Q.; Dunn, E. T.; Grandmaison, E. W.; Goosen, M. F. A. In *Applications of Chitin and Chitosan*.; Goosen, M. F. A., Ed.; Technomic Publishing Co.: Lancaster, 1997; pp 3−29.

(7) Kristl, J.; Smidkorbar, J.; Struc, E.; Schara, M.; Rupprecht, H. *Int. J. Pharm.* **1993**, *99*, 13−19.
(8) Alexeev, V. L.; Evmenenko, G. A. *J. Polym. Sci., Ser. A* **1999**, *41*, 966−974. Evmenenko, G. A.; Alexeev, V. L. *J. Polym. Sci., Ser. A* **1997**, *39*, 440−445.
(9) Peter, M. G. *J. Macromol. Sci., Pure Appl. Chem.* **1995**, *A32*, 629−640.
(10) Hwang, J. K.; Hong, S. P.; Kim, C. T. *J. Food Sci. Nutr.* **1997**, *2*, 1−5.
(11) Roberts, G. A. F.; Domszy, J. G. *Int. J. Biol. Macromol.* **1982**, *4*, 374−377.
(12) Steffe, J. F. *Rheological Methods in Food Process Engineering*; Freeman Press: East Lansing, MI, 1992.
(13) Knorr, D. *Food Technol.* **1984**, *38*, 85−97.
(14) Vorlop, K. D.; Klein, J. *Biotechnol. Lett.* **1981**, *3*, 9−14.
(15) Lowack, K.; Helm, C. A. *Macromolecules* **1998**, *31*, 823−833.
(16) See e.g.: Dahlgren, M. *Langmuir* **1994**, *10*, 1580. Claesson, P.; Mlomberg, E.; Froberg, J. C.; Nylander, T.; Arnebrandt, T. *Adv. Colloid Interface Sci.* **1995**, *57*, 161 and references therein.
(17) Gong, J.; Higa, M.; Iwasaki, Y.; Katsuyama, Y.; Osada, Y. *J. Phys. Chem. B* **1997**, *101*, 5487−5489.
(18) Kurokawa, T.; Gong, J.; Osada, Y. *Macromolecules* **2002**, *35*, 8161−8166.
(19) Bell, R. N., Ed.; *Sodium Metaphosphates*; McGraw-Hill: New York, 1950; Vol. III.
(20) Klein, J.; Kumacheva, E. *J. Chem. Phys.* **1998**, *108*, 6996−7009.
(21) Homola, A. M.; Israelachvili, J. N.; Gee, M. L.; McGuiggan, P. M. *J. Tribol.* **1989**, *111*, 675−682.
(22) Tabor, D.; Winterton, R. H. *Proc. R. Soc. London A* **1969**, *312*, 435−450.
(23) Raviv, U.; Laurat, P.; Klein, J. *Nature (London)* **2001**, *413*, 51−54.
(24) Derjaguin, B. V.; Churaev, N. V.; Muller, V. M. *Surface Forces*; Plenum Publishing Corp.: New York, 1987.
(25) Pashley, R. M. *J. Colloid Interface Sci.* **1981**, *80*, 153−162.
(26) Klein, J.; Luckham, P. F. *Macromolecules* **1984**, *17*, 1041−1048.
(27) Taunton, H. J.; Toprakcioglu, C.; Fetters, L. J.; Klein, J. *Macromolecules* **1990**, *23*, 571.
(28) Israelachvili, J. N. *J. Colloid Interface Sci.* **1973**, *44*, 259−272.
(29) Ligler, F. S.; Lingerfelt, B. M.; Price, R. P. *Langmuir* **2001**, *17*, 5082−5084.
(30) Fleer, G. J.; Cohen-Stuart, M. A.; Scheutjens, J. M. H. M.; Cosgrove, T.; Vincent, B. *Polymers at Interfaces*; Chapman and Hall: London, 1993.
(31) de Gennes, P. G. *Macromolecules* **1981**, *14*, 1637−1644.
(32) Luckham, P. F.; Klein, J. *J. Chem. Soc., Faraday Trans. 1* **1984**, *80*, 865−878.
(33) Klein, J.; Luckham, P. F. *Macromolecules* **1984**, *17*, 1041−1048.
(34) Raviv, U.; Tadmor, R.; Klein, J. *J. Phys. Chem. B* **2001**, *105*, 8125−8134.
(35) Raviv, U.; Giasson, S.; Kampf, N.; Gohy, J.; Jerome, R.; Klein, J. *Nature (London)* **2003**, *425*, 163−165.
(36) Plunkett, M. A.; Feiler, A.; Rutland, M. W. *Langmuir* **2003**, *19*, 4180−4187.
(37) Raviv, U.; Klein, J. *Science* **2002**, *297*, 1540−1543.
(38) Klein, J. *Annu. Rev. Mater. Sci.* **1996**, *26*, 581−612.
(39) Proc. Inst. Mech. Eng. Part H: Engineering in Medicine, 1987; Vol. 210: Special Issue on Biolubrication.
(40) Raviv, U.; Laurat, P.; Klein, J. *J. Chem. Phys.* **2002**, *116*, 5167−5172.

MA0303263